A Variational Method for the Analysis of Three-Dimensional Wind Fields from Two Doppler Radars

JIDONG GAO AND MING XUE

Center for Analysis and Prediction of Storms, University of Oklahoma, Norman, Oklahoma

ALAN SHAPIRO AND KELVIN K. DROEGEMEIER

Center for Analysis and Prediction of Storms and School of Meteorology, University of Oklahoma, Norman, Oklahoma

ABSTRACT

This paper proposes a new method of dual-Doppler radar analysis based on a variational approach. In it, a cost function, defined as the distance between the analysis and the observations at the data points, is minimized through a limited memory, quasi-Newton conjugate gradient algorithm with the mass continuity equation imposed as a weak constraint. The analysis is performed in Cartesian space.

Compared with traditional methods, the variational method offers much more flexibility in its use of observational data and various constraints. Using the radar data directly at observation locations avoids an interpolation step, which is often a source of error, especially in the presence of data voids. In addition, using the mass continuity equation as a weak instead of strong constraint avoids the error accumulation and the subsequent somewhat arbitrary adjustment associated with the explicit vertical integration of the continuity equation.

The current method is tested on both model-simulated and observed datasets of supercell storms. It is shown that the circulation inside and around the storms, including the strong updraft and associated downdraft, is well analyzed in both cases. Furthermore, the authors found that the analysis is not very sensitive to the specification of boundary conditions and to data contamination. The method also has the potential for retrieving, with reasonable accuracy, the wind in regions of single-Doppler radar coverage.

1. Introduction

Doppler radar has long been a valuable observational tool in meteorology. It has the capability of observing, at high spatial and temporal resolution, the internal structure of storm systems from remote locations. However, the direct measurements are limited to reflectivity, the radial component of velocity, and the spectrum width: there is no direct measurement of the complete three-dimensional (3D) wind field. In order to gain a more complete understanding of the atmosphere, it is desirable to know the full wind field.

When an atmospheric volume is observed simultaneously by two noncollocated Doppler radars, two degrees of freedom of 3D wind vectors are determined. Techniques have been developed since the late 1960s to produce so-called dual-Doppler analyses. These techniques can be divided into two categories in term of the analysis geometry: 1) those in cylindrical coordinates, and 2) those in Cartesian space. Early dual-Doppler analyses stressed the synthesis of two independent Doppler velocity estimates in cylindrical coordinates (e.g., Armijo 1969; Lhermitte and Miller 1970; Miller and Strauch 1974). Doviak et al. (1976) performed a detailed error evaluation applicable to these dual-Doppler analyses. To improve vertical velocity estimates, Ziegler (1978) proposed a variational dual-Doppler analysis to deal with the problem of the upper boundary condition.

Many other dual-Doppler synthesized analyses were performed directly in the Cartesian coordinate system. Brandes (1977) used a dual-Doppler analysis scheme in which wind components were synthesized from Doppler observations directly within a Cartesian grid, bypassing analysis procedures in cylindrical coordinates. Ray et al. (1980, 1981) designed a system to analyze data from multiple Doppler radars and tested it on a dataset acquired by two to four radars during a field experiment over Oklahoma. It used a variational adjustment to improve vertical velocity estimates based on the mass continuity equation. Recently, Sun and Crook (1997, 1998) used the adjoint approach to do the dual analyses and microphysical retrieval. They tested the method using both simulated data and real data. Although this is an exciting development,

Corresponding author address: Dr. Jidong Gao, Center for Analysis and Prediction of Storms, Sarkeys Energy Center, Suite 1110, 100 East Boyd, Norman, OK 73019.
E-mail: jdgao@ou.edu

their computational requirements may currently prohibit their use in an operational setting. Compared to those methods solved in cylindrical (COPLAN) coordinates, the Cartesian methods require only one interpolation. Further, the grid may be aligned in the cardinal directions regardless of the orientation of the radar system.

The dual-Doppler analysis methods have greatly aided our understanding weather phenomena ranging from mesoscale convective complexes to clear air boundary layers (e.g., Brandes 1977; Ray et al. 1981; Reinking et al. 1981; Carbone 1983; Kessinger et al. 1987; Parsons and Kropfli 1990; Atkins et al. 1995; Dowell and Bluestein 1997). However, they still suffer from notable deficiencies, including the setting of vertical velocity boundary conditions, spatial interpolation errors, discretizations, uncertainties in radial wind estimates (due to sidelobes and ground clutter), and the nonsimultaneous nature of the measurements. These problems have been discussed in Miller and Strauch (1974), Ray et al. (1975), Ray et al. (1980), Gal-Chen (1982), Testud and Chong (1983), Chong et al. (1983a,b), Ziegler et al. (1983), and Shapiro and Mewes (1999).

The most pronounced difficulties concern the vertical velocity boundary condition and interpolation procedure. The natural boundaries for the problem are the irregular boundaries of the data region itself. If the region of dual-Doppler data coverage extends all the way to the ground, then the impermeability condition could be safely applied. Unfortunately, the lower data boundary often lies hundreds to thousands of meters above ground level, where it is often inappropriate to apply the impermeability condition directly.

When the analysis is performed in a COPLAN coordinate system, it usually includes two steps: interpolation from a spherical coordinate system to a COPLAN coordinate system, and interpolation from a COPLAN coordinate system to a Cartesian coordinate system after the analysis is completed. Because of the irregular spatial distribution of the radar observations, large intervals between elevation angles [as large as 5°–6° for Weather Surveillance Radar–1988 Doppler (WSR-88D) radar data], and the presence of bad data values, significant error can be introduced in the interpolation processes.

In the present paper, a new technique, based on a variational approach, permits flexible use of radar data in combination with other observations as well as the use of various constraints through the definition a cost function. In particular, by applying the anelastic mass conservation equation as a weak constraint, the severe error accumulation in the vertical velocity can be reduced because the explicit integration of anelastic continuity equation is avoided.

In addition, this method combines interpolation and analysis into a single step. The analysis is performed more naturally and directly in a Cartesian coordinate system, only interpolation from regular Cartesian grid to irregular radar observation points is needed. Since this interpolation process is usually well defined, the error should be smaller than when interpolation is done from an irregular radar coordinate system to a regular Cartesian coordinate system (Gao et al. 1995). Further, this reverse interpolation procedure preserves the radial nature of radar observations.

This paper is organized as follows: in section 2, the variational method is introduced and a traditional dual-Doppler observation synthesis method is reviewed for reference. In section 3, the variational method is tested on a set of idealized data sampled from a simulated supercell storm for which the true wind field is known. In section 4, we apply this variational method to a dual-Doppler dataset from a tornadic supercell storm that occurred on 17 May 1981 near Arcadia, Oklahoma. Finally, a summary and concluding remarks are given in section 5.

2. Description of methodology

a. A variational dual-Doppler analysis method

Variational analysis is a procedure that minimizes a cost function J defined here to be the sum of squared errors due to the misfit between observations and analyses subject to constraints. Each constraint is weighted by a factor that accounts for its accuracy. There are different forms of J that might be considered, and each one of them will give a different result for the best-fit model solution. The variational method makes use of the derivative of J with respect to the analysis variables and J must therefore be differentiable. In our dual-Doppler radar analysis, we define the cost function as follows:

$$J = J_O + J_B + J_D + J_S, \tag{1}$$

$$J_O = \frac{1}{2} \sum_{m,n} \lambda_{m,n} (\mathbf{C}\mathbf{V}_r^{m,n} - \mathbf{V}_{\text{rob}}^{m,n})^2, \tag{2}$$

$$J_B = \frac{1}{2}\left[\sum_{ijk} \lambda_{ub}(\mathbf{u} - \mathbf{u}_b)^2 + \sum_{ijk} \lambda_{vb}(\mathbf{v} - \mathbf{v}_b)^2 \right. $$
$$\left. + \sum_{ijk} \lambda_{wb}(\mathbf{w} - \mathbf{w}_b)^2 \right], \tag{3}$$

$$J_D = \frac{1}{2} \sum_{ijk} \lambda_D \mathbf{D}^2, \tag{4}$$

$$J_S = \frac{1}{2}\left[\sum_{ijk} \lambda_{us}(\nabla^2 \mathbf{u})^2 + \sum_{ijk} \lambda_{vs}(\nabla^2 \mathbf{v})^2 \right. $$
$$\left. + \sum_{ijk} \lambda_{ws}(\nabla^2 \mathbf{w})^2 \right]. \tag{5}$$

Here J_O is the difference between the analyzed radial velocity $\mathbf{V}_r^{m,n}$ [elements are $\mathbf{V}_r^{m,n} = (xu + yv + zw)/r$] and the observed radial velocity $\mathbf{V}_{\text{rob}}^{m,n}$; m is the number of radars; n is the number of observations; $\mathbf{C}$ is a linear interpolation operator that maps $\mathbf{V}_r^{m,n}$ from the grid (Cartesian coordinates) to observation points (spherical coordinates);

and **u**, **v**, and **w** are wind components in Cartesian coordinates (x, y, z). Also, the square notation denotes the product of the transpose of a column vector with the vector and $\nabla^2\mathbf{u}$ denotes the vector whose elements are values of the Laplacian of u at grid points. It should be pointed out that the cost function can include other observations that directly or indirectly measure u, v, and w. They include soundings, single-level surface observations, aircraft data, or even satellite observations.

The second term of the cost function, J_B, measures how close the variational analysis is to the background fields. The third term, J_D, imposes a weak anelastic mass constraint on the analyzed wind field,

$$ D = \frac{\partial \overline{\rho} u}{\partial x} + \frac{\partial \overline{\rho} v}{\partial y} + \frac{\partial \overline{\rho} w}{\partial z}, \qquad (6) $$

where $\overline{\rho}$ is the mean air density in the horizontal level. The last term in the cost function, J_S, is a smoothness constraint.

Note that in the cost function, there exist several coefficients such as λ_{us}, λ_{vs}, and λ_{ws} that are commonly referred to as penalty constants. Some of these scalar coefficients correspond to matrices used in general data assimilation methods. In storm-scale data assimilation, especially with radar data, the matrix coefficients are usually difficult to obtain.

One of the major challenges of variational methods is the specification of the λ's. For our purpose, these coefficients are chosen according to the relative importance of each term. Experience with the test cases presented herein suggests that the solutions obtained are not very sensitive to the precise values of the λ's, and therefore it is appropriate to treat the λ's as tuning parameters. Typically, the analysis changes by only a small amount when a particular λ is halved or doubled, but the minimizing analysis does change as expected for large changes in the λ's (Hoffman 1984).

To solve the above variational problem by direct minimization, we need to derive the gradient of the cost function with respect to the control variables (u, v, and w). Taking the variation with respect to u, v, and w, we obtain the components of the gradient of J as follows:

$$ \left(\frac{\partial J}{\partial \mathbf{u}}\right)_{ijk} = \lambda_{m,n} \mathbf{C}^* \left(\frac{x}{r}\right) (\mathbf{C}\mathbf{V}_r^{m,n} - \mathbf{V}_{\text{rob}}^{m,n}) + \lambda_{ub}(\mathbf{u} - \mathbf{u}_b) $$

$$ - \lambda_D \overline{\rho} \frac{\partial \mathbf{D}}{\partial x} + \lambda_{su} \nabla^2(\nabla^2 \mathbf{u}), \qquad (7) $$

$$ \left(\frac{\partial J}{\partial \mathbf{v}}\right)_{ijk} = \lambda_{m,n} \mathbf{C}^* \left(\frac{y}{r}\right) (\mathbf{C}\mathbf{V}_r^{m,n} - \mathbf{V}_{\text{rob}}^{m,n}) + \lambda_{vb}(\mathbf{v} - \mathbf{v}_b) $$

$$ - \lambda_D \overline{\rho} \frac{\partial \mathbf{D}}{\partial y} + \lambda_{sv} \nabla^2(\nabla^2 \mathbf{v}), \qquad (8) $$

$$ \left(\frac{\partial J}{\partial \mathbf{w}}\right)_{ijk} = \lambda_{m,n} \mathbf{C}^* \left(\frac{z}{r}\right) (\mathbf{C}\mathbf{V}_r^{m,n} - \mathbf{V}_{\text{rob}}^{m,n}) + \lambda_{wb}(\mathbf{w} - \mathbf{w}_b) $$

$$ - \lambda_D \overline{\rho} \left(\frac{\partial \mathbf{D}}{\partial z}\right) + \lambda_{sw} \nabla^2(\nabla^2 \mathbf{w}). \qquad (9) $$

Here, $\mathbf{C}^*$ is the adjoint of operator $\mathbf{C}$. In the above, the commutation formula

$$ \sum \zeta \boldsymbol{\nabla} \eta = - \sum \eta \boldsymbol{\nabla} \zeta \qquad (10) $$

of the finite-difference analog is used (Sasaki 1970), where we have specified values of u, v, w at the boundaries; that is,

$$ \delta u = \delta v = \delta w = 0. \qquad (11) $$

(Note: in coding the program, the derivations above are performed in its finite-difference analog. For clarity, we write them here in their continuous form.) It can be also noted that setting the gradients $\partial J/\partial \mathbf{u}$, $\partial J/\partial \mathbf{v}$, $\partial J/\partial \mathbf{w}$ in (7)–(9) to zero yields three coupled Euler–Lagrange equations.

After the gradients of cost function are obtained, the problem can be solved in the following way.

- Choose the first guess of control variable $\mathbf{Z} = (u, v, w)^{\text{T}}$ (in our experiment, all first guesses are zero).
- Calculate the cost function according to Eqs. (1)–(5).
- Calculate the gradients $\partial J/\partial \mathbf{u}$, $\partial J/\partial \mathbf{v}$, and $\partial J/\partial \mathbf{w}$ according to Eqs. (7)–(9).
- Use a conjugate gradient method (Navon and Legler 1987) to obtain update values of control variables

$$ \mathbf{Z}_{ijk}^{(n)} = \mathbf{Z}_{ijk}^{(n-1)} + \alpha \cdot f(\partial J/\partial \mathbf{Z})_{ijk}, \qquad (12) $$

where n is the number of iterations, α is an optimal step size, obtained by the so-called line search process in the optimal control theory (Gill et al. 1981), and $f(\partial J/\partial \mathbf{Z})_{ijk}$ is the optimal descent direction obtained by combining the gradients from several former iterations.

- Check if the optimal solution has been found by computing the norm of the gradients or the value of J to see if it is less than a prescribed tolerance. If the criterion is satisfied, stop iterating and output the optimal u, v, and w.
- If the convergence criterion is not satisfied, steps 2 through 5 are repeated using updated values of u, v, and w as the new guess. The iteration process is continued until a satisfactory solution is found.

b. Conventional synthesis method

To highlight the differences between traditional dual-Doppler analysis approaches and our variational analysis method, the procedure of a traditional method is briefly reviewed here. It follows closely the widely used dual-Doppler analysis technique contained in the Na-

tional Center for Atmospheric Research (NCAR) software package CEDRIC (Mohr 1988).

The radial velocity V_r at a point (X, Y, Z) can be expressed as

$$V_{rP} = uX_P + vY_P + wZ_P, \qquad (13)$$

where

$$X_P = \frac{x - x_P}{R_P}, \qquad Y_P = \frac{y - y_P}{R_P}, \qquad Z_P = \frac{z - z_P}{R_P},$$

$$R_P = (x - x_P)^2 + (y - y_P)^2 + (z - z_P)^2, \quad \text{and} \quad (14)$$

$u, v,$ and w are the Cartesian velocity components (Mohr 1988). This notation is used to conform to that for traditional ground-based dual-Doppler analysis.

For two radars, we let P be A and B, respectively, and we obtain the following formula from (13) and (14):

$$u = \frac{V_{rA}Y_B - V_{rB}Y_A}{D} + \varepsilon_u w, \qquad (15)$$

$$v = \frac{V_{rB}X_A - V_{rA}X_B}{D} + \varepsilon_v w, \qquad (16)$$

where $D = X_A Y_B - X_B Y_A$, $\varepsilon_u = (Y_A Z_B - Y_B Z_A)/D$, and $\varepsilon_v = (X_B Z_A - X_A Z_B)/D$. With data from only two radars, $u, v,$ and w are not explicitly determined. But for a good "first guess," the w terms can be neglected, yielding the following estimates for the horizontal velocities:

$$u' = \frac{V_A Y_B - V_B Y_A}{D}, \qquad (17)$$

$$v' = \frac{V_B X_A - V_A X_B}{D}. \qquad (18)$$

The factors ε_u and ε_v become geometric multipliers that can be used to adjust the estimates u' and v' if w is found using other information.

The vertical velocity estimate is usually obtained by integrating the anelastic mass continuity equation (6) upward (or downward) subject to the boundary condition $w = 0$ at the lower boundary (or upper boundary). A wind adjustment (O'Brien 1970) is typically applied to ensure that $w = 0$ at both boundaries. The horizontal velocity components are then recomputed as

$$u = u' + \varepsilon_u w, \qquad (19)$$

$$v = v' + \varepsilon_v w. \qquad (20)$$

With this simple approach, the velocities are calculated and corrected by an iterative procedure. First, an approximate w is obtained by integrating the continuity equation (based on the approximate horizontal velocities). The horizontal velocities are then corrected, and the process is repeated until a convergence criterion is met.

c. The effect of terminal velocity

With both variational and traditional methods, the fall speed of precipitation has to be taken into account. For radar scans at a nonzero elevation angle, the fall speed of precipitation particles contributes to the Doppler estimate of radial velocity. The observations of radial velocity are adjusted to remove this contribution, using (Foote and duToit 1969; Atlas et al. 1973)

$$v_r = v'_r + w_t \sin\theta, \qquad (21a)$$

where v_r is the air radial velocity, v'_r is the target radial velocity, w_t is the terminal velocity of precipitation, and θ is the elevation angle ($0°$ is horizontal).

The adjustment to radial velocity in Eq. (21a) is based on an empirical relationship between reflectivity factor and raindrop terminal fall velocity (Atlas et al. 1973):

$$w_t = 2.65\left(\frac{\rho_0}{\rho}\right)Z^{0.114}. \qquad (21b)$$

Here Z is the reflectivity, ρ the air density, and ρ_0 the air density at the surface.

3. Tests with simulated data

a. Experimental design

To evaluate the performance of our variational analysis method and compare it with the more traditional method outlined in the previous section, we utilize a set of simulated dual-Doppler data. This strategy is often called the observation system simulation experiment (OSSE). A well-documented tornadic supercell storm that occurred near Del City, Oklahoma, on 20 May 1977 is used for the numerical experiments. This storm has been studied extensively, using both multiple Doppler analysis and numerical simulation. For details on its morphology and evolution, readers are referred to Ray et al. (1981), Klemp et al. (1981), and Klemp and Rotunno (1983).

The Advanced Regional Prediction System (ARPS; Xue et al. 1995) is used here to perform a 2-h simulation of this storm. The simulation starts from a thermal bubble placed in a horizontally homogeneous base state specified from the sounding used in Klemp et al. (1981). As in Klemp et al. (1981), a mean storm speed (U = 3 m s^{-1}, V = 14 m s^{-1}) is subtracted from the sounding to keep the right-moving storm near the center of the model domain.

The model grid comprises $67 \times 67 \times 35$ grid points, and the grid interval is 1 km in the horizontal and 0.5 km in the vertical. The physical domain size is $64 \times 64 \times 16$ km^3. The storm is initiated by an isolated thermal bubble centered at $x = 48$ km, $y = 16$ km, and $z = 1.5$ km, with the origin at the lower-left corner of the grid. The radius of the bubble is 10 km in both the x and y directions and 1.5 km in the vertical direction. The magnitude of the thermal perturbation is $4°$. Kessler (1969) warm rain microphysics is used together with a 1.5-order turbulent kinetic energy subgrid parameterization. Open boundary conditions are used at the lateral boundaries while an upper-level Rayleigh damping layer
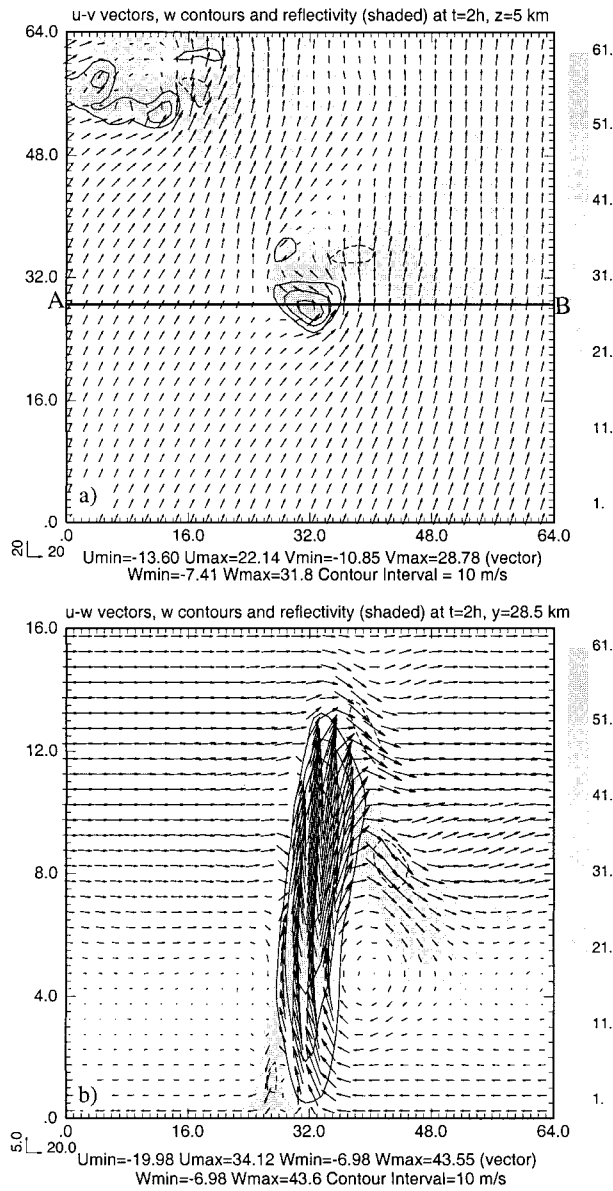
u-v vectors, w contours and reflectivity (shaded) at t=2h, z=5 km

Umin=-13.60 Umax=22.14 Vmin=-10.85 Vmax=28.78 (vector)
Wmin=-7.41 Wmax=31.8 Contour Interval = 10 m/s

u-w vectors, w contours and reflectivity (shaded) at t=2h, y=28.5 km

Umin=-19.98 Umax=34.12 Wmin=-6.98 Wmax=43.55 (vector)
Wmin=-6.98 Wmax=43.6 Contour Interval=10 m/s

FIG. 1. The ARPS model-simulated wind vectors, vertical velocity
w (contours), and simulated reflectivity (shaded) fields of the 20 May
1977 supercell storm at 2 h: (a) horizontal cross section at $z = 5$ km
and (b) vertical cross section at $y = 28.5$ km, i.e., through line A–B
in (a).

is included to reduce wave reflection from the top of
the model.

By 2 h into the simulation, the initial storm has un-
dergone a splitting process (Klemp and Wilhelmson
1978), with the right mover remaining near the center
of the domain and the left mover propagating to the
northwest corner. Figure 1 shows horizontal and vertical
cross sections of wind, vertical velocity (vertical section
is plotted through line A–B in Fig. 1a), and reflectivity
fields at 2 h. A strong rotating updraft (with maximum
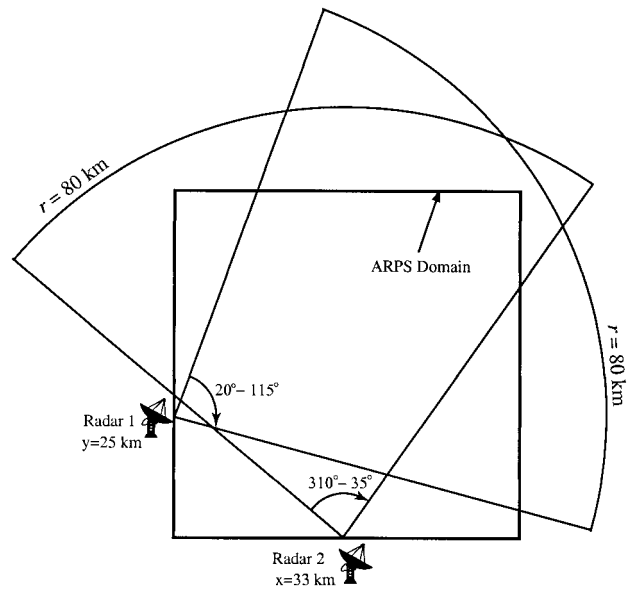vertical velocity exceeding 34 m s^{-1}) and associated

FIG. 2. Locations of the two assumed radars that sample data from
the ARPS 2-h run in Fig. 1.

low-level downdraft are evident near the center of the
domain while disturbances associated with the left mov-
er are also clear. Downstream of the overshooting up-
draft at the tropopause level are downward returning
flows that exhibit gravitational oscillations (Fig. 1b).
The evolution of the simulated storm is qualitatively
similar to that described by Klemp and Wilhelmson
(1981) and, by 2 h, has attained a structure typical of
mature supercell storms.

The simulated 3D convective-scale wind field at 2 h
is sampled by two pseudoradars, the locations of which
relative to the grid are shown in Fig. 2. The wind com-
ponents are first interpolated using a Cressman scheme
(1959) from the model grid points to the sampling lo-
cations along the radar beams with the influence radius
$R = 2.5$ km, and are synthesized to obtain radial ve-
locities according to Eq. (13). The elapsed times for the
volume scans of two radars are neglected, and thus we
presume that the radial wind observations are simulta-
neous.

Radar 1 in Fig. 2 covers a horizontal area of 10 km
$< r < 80$ km and $20° < \alpha < 115°$, where r is the radius
and α is the azimuthal angle. Radar 2 covers a horizontal
area of 10 km $< r < 80$ km and $310° < \alpha < 360° +
35°$. The gate spacing is 500 m, the azimuthal angle is
1°, and the elevation angle is 1°. The lowest elevation
angle is 0.5°. The simulated data are only specified in
precipitation regions (where reflectivity is greater than
zero) covered by both radars. In order to simulate the
radar's statistical error, random errors with different
magnitudes are added to the radial velocities in three of
the experiments.

To measure the accuracy of the dual-Doppler analysis,
we calculate the following error statistics.

TABLE 1. List of experiments with simulated dataset.

Experiments	Scheme	Number of iterations	Horizontal wind (V_H)			Vertical wind (w)		
			rms	rre	cc	rms	rre	cc
CNTL1	Control	50	4.893	0.257	0.968	2.626	0.786	0.657
CNTL2	Control	100	4.002	0.210	0.978	2.140	0.641	0.775
CNTL	Control	200	3.958	0.209	0.978	1.937	0.609	0.825
NOWC	No weak constraint	200	4.019	0.211	0.978	4.225	1.265	0.222
NOSM	No smoothness	200	4.557	0.240	0.971	2.631	0.788	0.712
ERR1	20% errors	200	5.356	0.282	0.960	2.572	0.808	0.729
ERR2	60% errors	200	5.572	0.306	0.954	2.757	0.825	0.707
ERR3	100% errors	200	8.237	0.434	0.910	3.948	1.241	0.544
ARCADIA	Variational	200	N.A.					

The rms error and relative rms error of the horizontal winds are given by

$$\mathrm{rmsv} = \left[\frac{\sum_{i=1}^{N}(u - u_{\mathrm{ref}})_i^2 + \sum_{i=1}^{N}(v - v_{\mathrm{ref}})_i^2}{2N}\right]^{1/2}, \quad \text{and} \quad (22)$$

$$\mathrm{rrev} = \left[\frac{\sum_{i=1}^{N}(u - u_{\mathrm{ref}})_i^2 + \sum_{i=1}^{N}(v - v_{\mathrm{ref}})_i^2}{\sum_{i=1}^{N}(u_{\mathrm{ref}})_i^2 + \sum_{i=1}^{N}(v_{\mathrm{ref}})_i^2}\right]^{1/2}. \quad (23)$$

And the rms error and relative rms error of the vertical velocities are likewise given by

$$\mathrm{rmsw} = \left[\frac{\sum_{i=1}^{N}(w - w_{\mathrm{ref}})_i^2}{N}\right]^{1/2}, \quad \text{and} \quad (24)$$

$$\mathrm{rrew} = \left[\frac{\sum_{i=1}^{N}(w - w_{\mathrm{ref}})_i^2}{\sum_{i=1}^{N}(w_{\mathrm{ref}})_i^2}\right]^{1/2}. \quad (25)$$
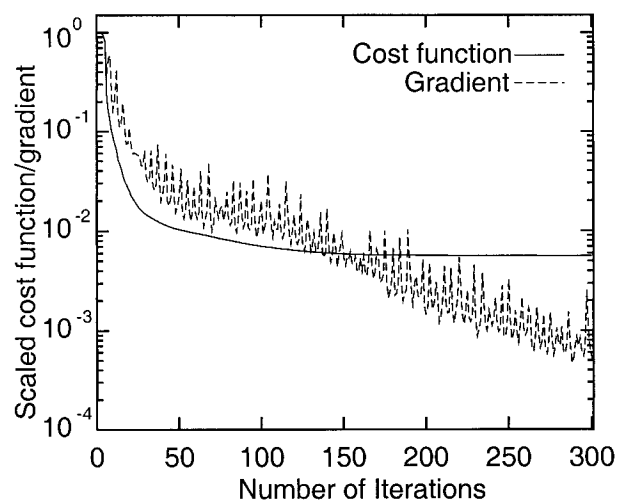

FIG. 3. The scaled cost function (J_k/J_o) and scaled gradient norm ($\|\mathbf{g}_k\|/\|\mathbf{g}_0\|$) as a function of the number of iterations.

Here N represents the total number of grid points for u, v, and w in the area covered by the two Doppler radars. The subscript ref stands for the reference or actual field from the ARPS model solution. In addition, the correlation coefficients (CC) of horizontal and vertical wind between the retrieved field (u, v, and w) and reference fields (u_{ref}, v_{ref}, and w_{ref}) are also calculated for each experiment.

b. Results of analysis

In this section, we present the results from a set of OSSE experiments outlined in the previous section. The analysis domain is the same as the ARPS integration domain described earlier, and the experiments are listed in Table 1. Among them is the control run (CNTL), the results of which are shown at three minimization iteration steps: 50, 100, and 200. Two more experiments are performed to examine the effect of a weak mass continuity constraint (NOMC) and spatial smoothing (NOSM). The perfect OSSE data are used for these experiments. Finally, experiments ERR1 through ERR3 test the error tolerance of the variational method by adding some errors to the OSSE data. The first guesses for all of the experiments are zero. The horizontally homogeneous background field is specified from a single sounding of 20 May 1997 at Del City, Oklahoma.

The parameter settings used are $\lambda_{m,n} = 1$, $\lambda_{ub} = \lambda_{vb} = 10^{-2}$, $\lambda_{wb} = 0.0$, $\lambda_D = 1/(0.5 \times 10^{-3})^2$, and $\lambda_{us} = \lambda_{vs} = \lambda_{ws} = 0.5 \times 10^{-3}$. These values are chosen so that the constraints are of roughly the same order of magnitude after being multiplied by the coefficients. These parameters also indicate the relative importance of each term in the cost function.

We first examine the number of iterations needed to minimize J. Generally speaking, the optimal number is case dependent and is also a function of the preconditioning and minimization method used. In practice, the appropriate number of iterations can be estimated by examining the behavior of cost function; that is, the minimization process can be stopped when the change in the cost function becomes small. Figure 3 shows that the cost function starts to level off after 100 iterations in the control experiment. From about 150–300 itera-

tions, the curve of cost function becomes essentially horizontal, although the norm of the gradient still decreases further.

The quality of the retrieval can be ascertained by the rms errors and correlation coefficients, and by comparing the retrieved fields with the "exact" solution from the ARPS model. The error statistics for various numbers of iterations are shown in Table 1. The rms errors and correlation coefficients for the horizontal wind change very little after 50 iterations; however, the vertical velocity retrieval continues to improve thereafter.

To examine the quality of the analysis more closely, we show in Figs. 4–5 sample plots for iteration steps 50 and 200, respectively. Comparing with the true fields in Fig. 1, all the features in the horizontal winds, that is, the curvature around the rotating updraft and the convergence, are well retrieved. However, the flow in the vertical cross section is significantly different in Figs. 4b–5b. Although the general structure of updraft is retrieved after only 50 iterations, the maximum vertical velocity is very low (21.62 m s^{-1}) compared to the "true" one (43.55 m s^{-1}). At middle and upper levels, the downdraft in the eastern part of the model domain is not present. Oscillations downstream of the updraft top due to gravitational waves are also missing. For iteration 100 (not shown), the maximum updraft is still low (30.12 m s^{-1}) and the downdraft at midlevels is retrieved. However, the downdraft at the upper levels is still missing. At 200 iterations, both the horizontal and vertical winds are well recovered (see Fig. 5). The analyzed 3D wind fields are reasonably close to the true wind fields in Fig. 1. The relative rms errors at this iteration step are less than that of the other two steps in Table 1. Thus, in the minimization process, the number of iterations needed to obtain a good retrieval, is very different for the horizontal and vertical winds.

To obtain the reasonable horizontal wind analysis, only a small number of iterations are needed. This is, because Doppler radars usually operate at low elevation angles, the horizontal winds are well observed. The absolute values of the gradient of the cost function with respect to horizontal winds for the first iteration are relatively large when compared to those for the vertical velocity (not shown). Hence, the cost function is more sensitive to horizontal winds than vertical winds, and therefore the horizontal wind component is easily retrieved with sufficient accuracy in only 50 iterations. The contribution of vertical velocity to the observed radial velocities is, however, relatively small due to the small elevation angles, and thus the analysis still contains large errors after first 50 iterations. After that, the absolute values of the gradient of the cost function with respect to horizontal and vertical winds become the same order of magnitude and the mass continuity constraint becomes effective. The vertical velocity becomes well retrieved after 200 iterations because of adjustments to this constraint giving better-retrieved horizontal winds. From iterations 200–300, the accuracy of both
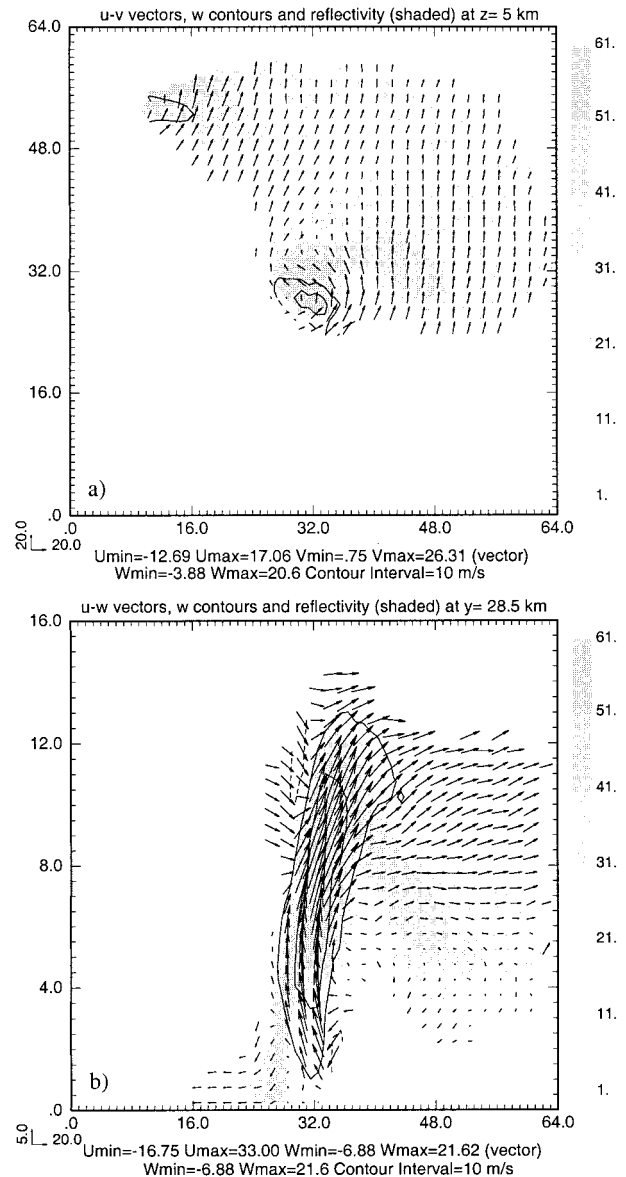

FIG. 4. Wind vectors and vertical velocity (contours) retrieved from data sampled by two Doppler radars (see Fig. 2) using the variational analysis method at iteration number 50. The horizontal cross section is at $z = 5$ km and vertical cross section at $y = 28.5$, as shown in Fig. 1 as line A–B. Also shown as shaded contours are the simulated reflectivity fields. Only analysis in the "rainy" areas (areas with reflectivity) are shown since those are where observations are available.

the horizontal and vertical wind remains essentially unchanged and thus we terminate the analysis after 200 iterations.

c. The role of the anelastic mass continuity constraint

Our variational analyses show satisfactory results of 3D dual-Doppler wind analysis, including the vertical velocity. To explain the role of the weak mass continuity
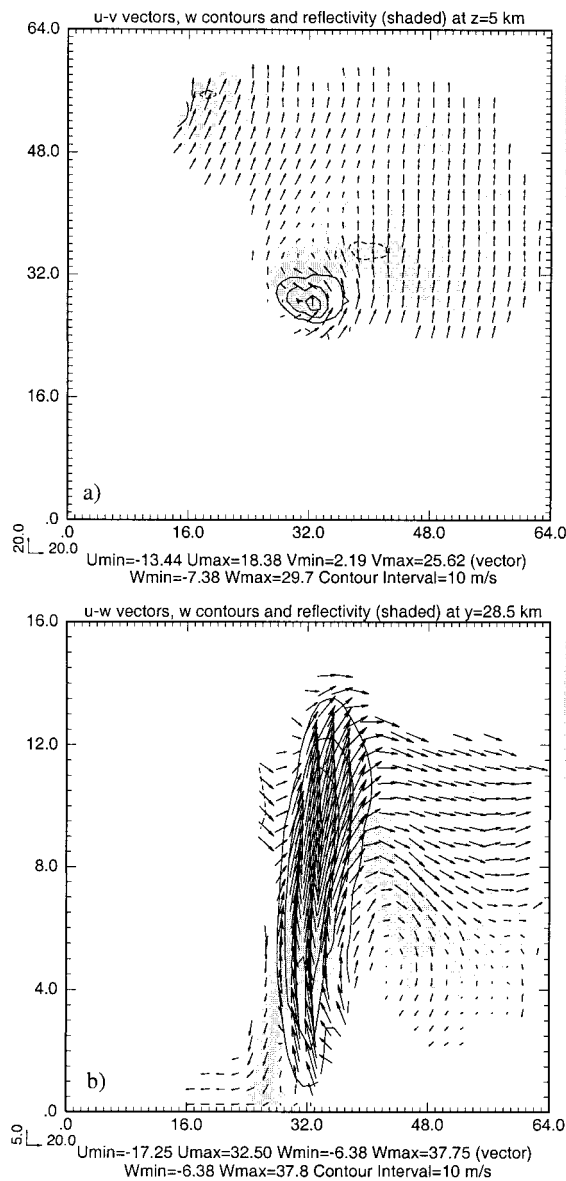
FIG. 5. Wind vectors and vertical velocity (contours) retrieved from data sampled by two Doppler radars (see Fig. 2) using the variational analysis method at iteration number 200. The location of cross sections and plotting convections are the same as in Fig. 4.

FIG. 6. As in Fig. 5 but for experiment NOWC, which excludes the mass-continuity weak constraint.

constraint, we perform experiment NOWC (see Table 1), which is exactly the same as CNTL except that the mass continuity constraint is removed.

As shown in Table 1, both the rms error and correlation coefficients indicate that the horizontal wind is recovered with reasonable accuracy; however, the retrieval of vertical velocity is poor. Figure 6b shows that no coherent structure in w is retrieved below 4 km, but results above 4 km are qualitatively good. This is not surprising, though, because very limited information on w is contained in the radial wind observations at low levels.
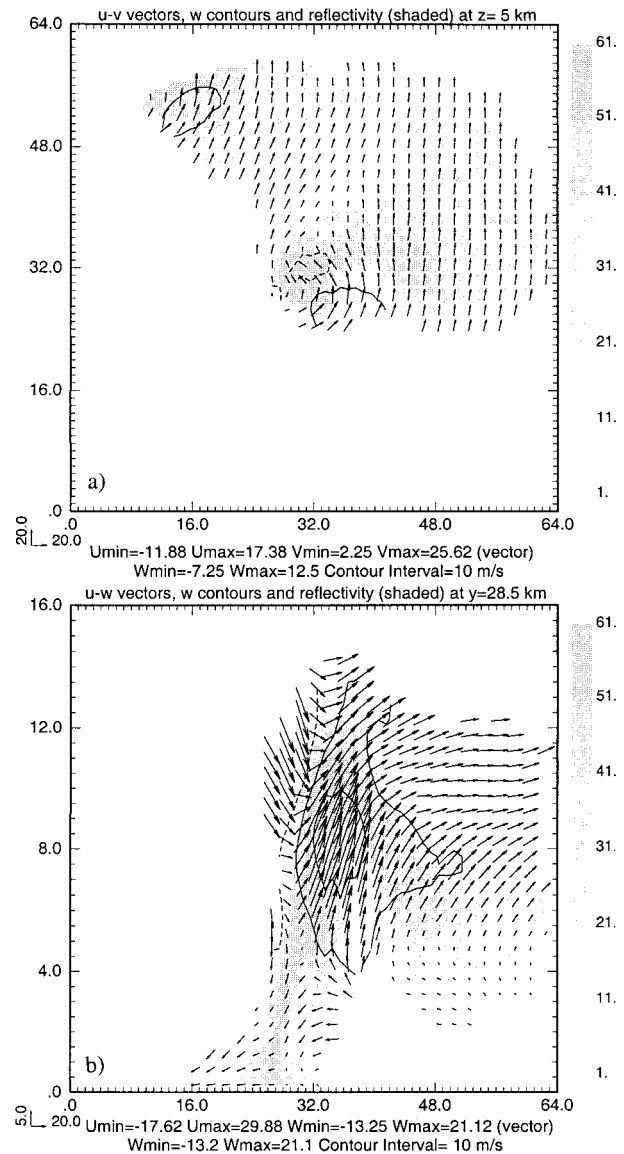
With conventional methods, the vertical velocity is obtained by integrating the mass continuity equation, and in this sense, the equation is used as a *strong constraint*. The main difficulty lies in specifying the w boundary conditions. The requirement of zero vertical velocity at the ground is the most natural physical condition (Miller and Strauch 1974; Doviak et al. 1976). However, it was later demonstrated that upward integration of vertical velocity was unreliable because the bias errors in the divergence field can be amplified exponentially with height (Ray et al. 1980).

To reduce the accumulation of w error, Ziegler (1978) proposed a dual-Doppler analysis that incorporated boundary conditions $w = 0$ at $z = 0$ and $w = -v_t$ at the upper data boundary (v_t terminal velocity, which

was small in his study). Further, Ray et al. (1980) applied a variational wind adjustment to the analyzed winds in their multiple-Doppler radar analysis. The anelastic mass continuity equation was used as a strong constraint in both cases.

The vertical integration of the anelastic mass continuity equation is particularly difficult for our simulated dataset because of the presence of large data-void areas. For example, the lower boundary of the radar echo is as high as 6 km in certain vertical columns (see Fig. 1b). The resultant w field from such integration can be very problematic even if an additional variational adjustment is applied. It is therefore advantageous to apply the mass continuity equation as a weak constraint so that explicit integration of the equation is avoided. By doing so, to specify w boundary conditions explicitly at data boundaries is not needed. However, the use of the background field and/or the smoothness constraint still permits us to set w equal to zero at both model top and bottom.

To summarize, in conventional dual-Doppler techniques, the horizontal and vertical winds are derived in two separate steps. With our method, the horizontal and vertical wind components are retrieved together, subject to the weak constraint of anelastic mass continuity. The use of a weak instead of strong constraint also leads to procedural simplicity in that the explicit solution of an elliptic equation that would arise from the use of a strong constraint is avoided. The latter tends to be sensitive to the specification of boundary conditions. This finding also agreed with that of Xu and Qiu (1994) who compared the advantages and disadvantages of using weak versus strong constraints of mass continuity in the so-called simple adjoint techniques.

d. The role of smoothing

In addition to the physical constraints, a smoothness constraint, J_s, as proposed by Thacker (1988), is added to the cost function J. Yang and Xu (1996) discussed theoretically the role and effect of a spatial smoothness constraint on statistical errors in variational data assimilation in their simple one-dimensional model. Sun and Crook (1994) found the accuracy of retrieval results can be greatly improved when a smoothness constraint was used in their experiments. Table 1 shows that, when this smoothness term is excluded from the cost function (experiment NOSM), the retrieval results deteriorate, especially for the vertical velocity. The analyzed 3D wind fields (Fig. 7) lack coherence and contain significant noise. From this test, the importance of smoothness is clear: The inclusion of the smoothness term improves the 3D wind analysis by removing small-scale noise and also helps to increase the area of influence of the radar data. The latter is more important in the vertical direction since the separation between observations is often large. For WSR-88D data, the scans can be more than several degrees apart in elevation angle.
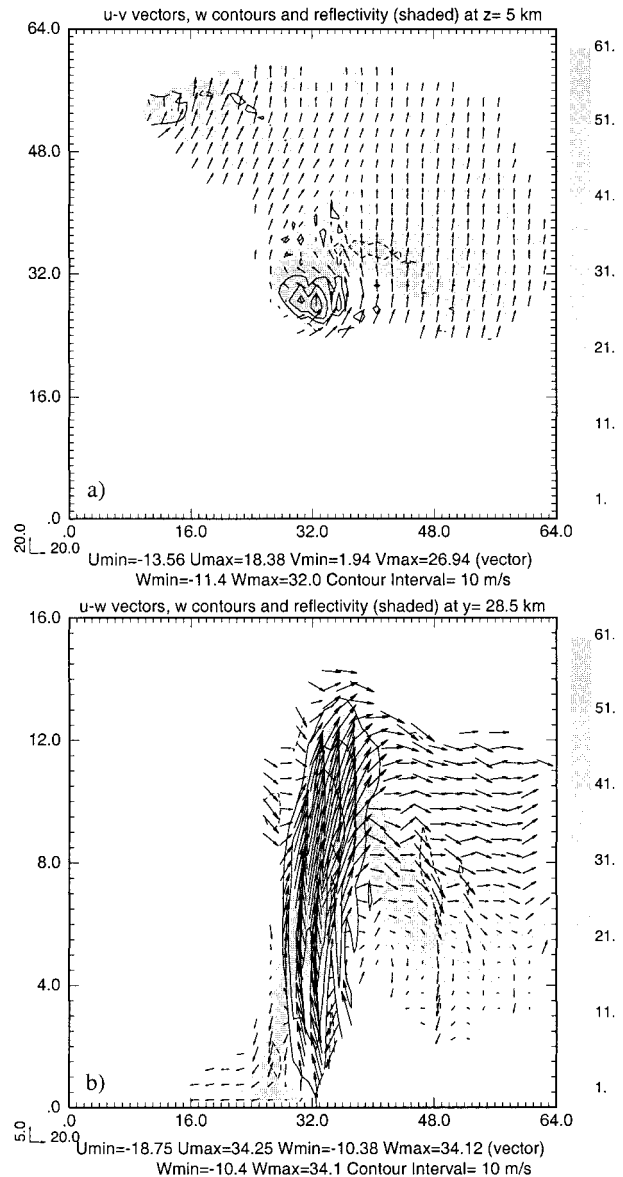

FIG. 7. As in Fig. 5 but for experiment NOSM, which excludes the smoothing terms in the cost function.

From Table 1, it can be seen that the relative impact of smoothing versus anelastic mass continuity equation on the horizontal wind field is about the same, but mass continuity is much more important than smoothing for vertical velocity. Lack of smoothing alone increases rms error for vertical velocity by about 0.7 m s^{-1} over the control run, but lack of mass continuity alone increases rms error for vertical velocity by about 3.3 m s^{-1}.

e. Relaxation to the background

When radar data are to be used to initialize a numerical weather prediction (NWP) model, a complete description of the wind and other meteorological vari-

ables is needed in the entire model domain. Even for diagnostic studies, consistent analysis outside the radar data areas is also desirable. Conventional observations such as the rawinsondes, or background fields from NWP models, can be used to complement the radar data. However, there is the issue of blending the radar data with the background information.

Lin et al. (1993) proposed a method for obtaining a smooth transition from regions with radar observations to the ambient environment defined by a single sounding. Using the analyzed u and v fields at the data boundaries as the *inner* Dirichlet boundary condition and a single rawinsonde as the *outer* Dirichlet boundary condition (i.e., on the domain boundary), they solved two Laplace equations for u and v that minimize the horizontal gradients of u and v in the data-void areas. Because the u and v fields so obtained do not satisfy mass continuity in general, they applied an additional mass continuity variational adjustment. Nevertheless, on the boundary between the original radar data and the filled data, the space derivatives of the wind field were discontinuous.

Ellis (1997) also used OSSE to study hole filling the data voids in simulated radar data. Two different hole-filling techniques were involved in his method: The first one was similar to that of Lin et al. (1993); the second one minimized the second derivative of the scalar field being filled. In both cases the variational wind adjustment of Ray et al. (1981) was then applied to the hole-filled wind field. He found the first technique performed generally better than the second one. The variational wind adjustment improves the statistics of each hole-filling wind field.

With the variational method proposed here, the several steps commonly used in conventional methods are effectively combined into a single step. The rawinsonde (and other available) data are incorporated into the cost function to automatically fill the data-void regions. The weighting constant for the background field should be properly selected, and should be large enough to keep the wind outside the precipitation regions close to the background, but not too large so as to lessen the fit of the analysis to radar observations. In our experiments, we find that $\lambda_{ub} = \lambda_{vb} = 10^{-2}$, $\lambda_{wb} = 0$ works well.

To examine the effectiveness of using a single sounding to specifying the background environment, we repeat the control experiment without the background sounding. The analyzed winds are plotted for the entire domain in Fig. 8 and compared with those of the control case, replotted for the same domain in Fig. 9. In the analysis without a background, no information is available outside the data areas, the analysis remains largely unchanged from the first guess, which in our case is zero (Fig. 8). However, for the control case, though no observational constraint is available outside the radar-observed data areas, the analysis takes on the values of the background and the transition is smooth between the data area and nondata area (Fig. 9). It is worth point-
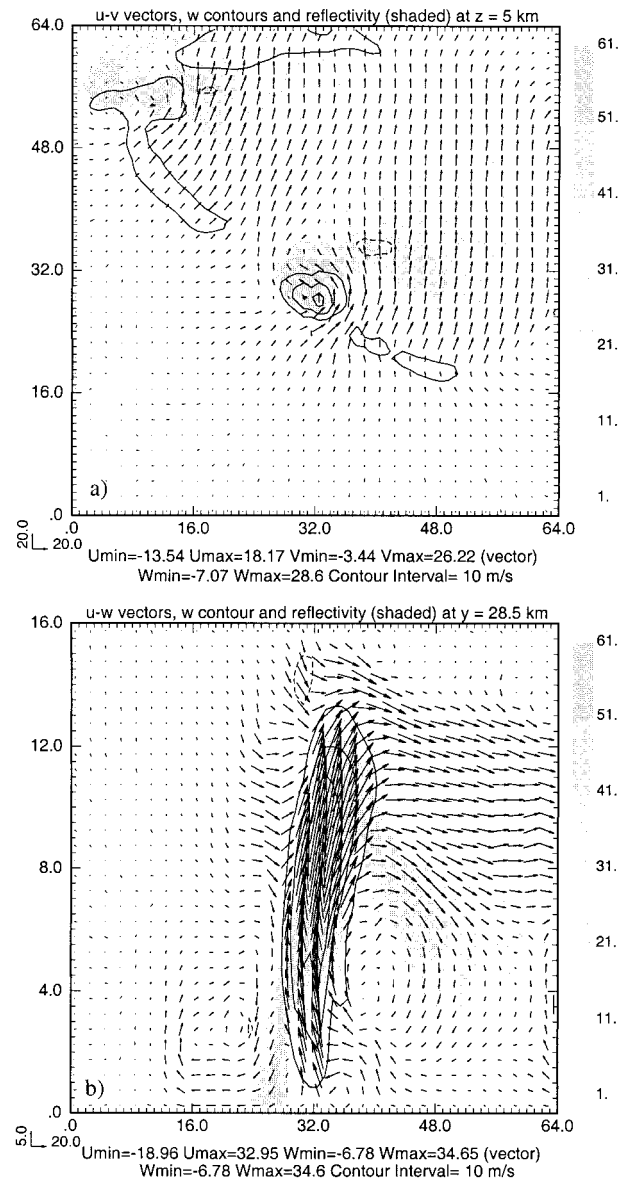

FIG. 8. As in Fig. 5 but for an experiment that does not include background (rawinsonde) data. The fields in the entire analysis domain are shown.

ing out that even though the analysis outside the radar data areas is very poor with strong horizontal convergence and divergence near the data boundaries, the analysis within the data coverage area is very good (cf. Fig. 8 and Fig. 9). This again suggests that the current variational analysis is not very sensitive to data boundaries and parameters specified outside the radar-observed storm region.

It is also interesting to note that near the northwest corner of the domain, the left-moving storm is partially covered by a single radar (radar 2 in Fig. 2). Our analysis procedure is still able to retrieve some of the flow structure of this storm cell. This is possible due to the fact
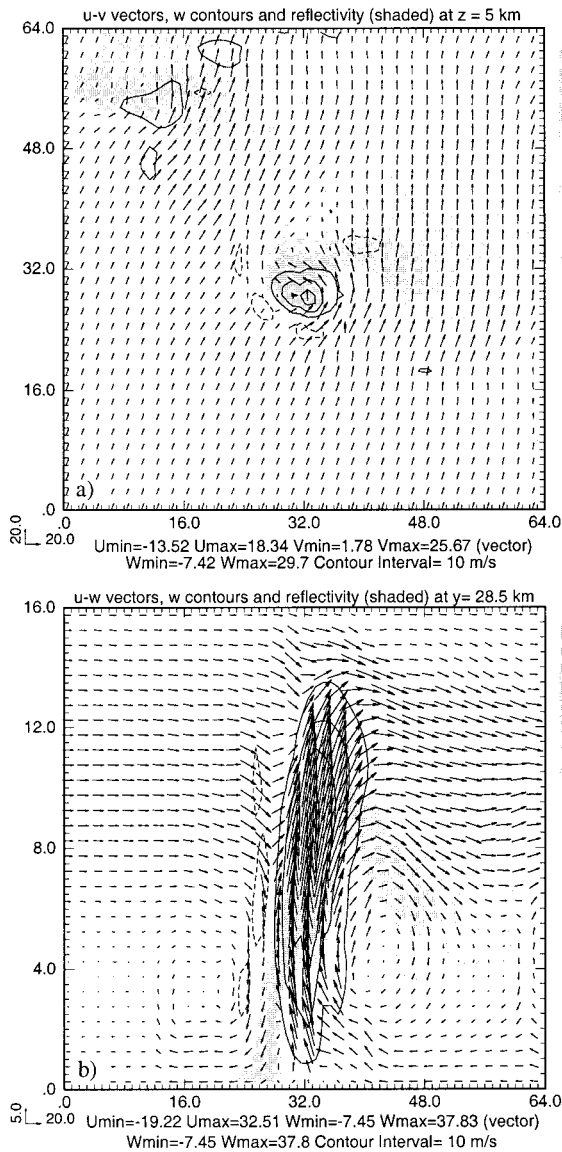
u-v vectors, w contours and reflectivity (shaded) at z = 5 km

Umin=-13.52 Umax=18.34 Vmin=1.78 Vmax=25.67 (vector)
Wmin=-7.42 Wmax=29.7 Contour Interval = 10 m/s

u-w vectors, w contours and reflectivity (shaded) at y= 28.5 km

Umin=-19.22 Umax=32.51 Wmin=-7.45 Wmax=37.83 (vector)
Wmin=-7.45 Wmax=37.8 Contour Interval = 10 m/s

FIG. 9. Same as in Fig. 5 except that the analyzed fields are shown for the entire analysis domain.

that, with variational methods, one can make use of whatever information is available, and often in an optimal way, whereas with traditional methods, dual-Doppler radar coverage is essential.

f. Sensitivity to random observational errors

In the above experiments we have assumed that the radial velocity observations are free of error. In reality, radial velocity observations can contain large errors, especially some biased errors (ground cluster, anomalous propagation, etc.). However, it is very difficult to account for simulated biased errors. In this section, we test the quality of the variationally analyzed fields subject to random observational errors. Experiments ERR1,

ERR2, and ERR3 (Table 1) involve the addition of 20%, 60%, or 100% random errors, respectively, to the radial velocity observations from both radars. In other words, we use $V_r' = (1 + \alpha\varepsilon)V_r$ as the observations, where ε represents uniformly distributed random numbers between -1 and $+1$ and α is 0.2, 0.6, and 1, respectively. When $\alpha = 0.2$, the relative rms error for the horizontal wind is not significantly changed from that of the control experiment (28% vs 20.9% for CNTL). However, the relative rms error of vertical velocity increases from 60.9% to 80.8%, and the correlation coefficient decreases from 0.825 to 0.729. Thus, the vertical velocity is more sensitive to observational errors than the horizontal wind. Nevertheless, the general features of the 3D wind field are well retrieved (Fig. 10).

When α is increased to 0.6, the retrieval of horizontal winds remains good, but the retrieved vertical velocity exhibits larger noise (figures not shown). In experiment ERR3, we give an extreme example by setting α to 1.0. This example shows that the method is rather robust even for such large observation errors. The relative rms error of the horizontal winds remains reasonably small (0.43) and the correlation coefficient is as high as 0.91 (Table 1). However, the relative errors of the vertical velocity are as large as 1.24.

Figure 11 shows considerable noise in both the horizontal and vertical wind fields. In spite of that, the general pattern of the flow is still rather similar to the pseudo-observations.

4. Application to real data

In the previous section, we discussed results from a set of OSSE experiments using model-generated pseudo-observations. To demonstrate the effectiveness of the variational method for real data, we apply our method to the 17 May 1981 Arcadia, Oklahoma, supercell storm. Twelve coordinated dual-Doppler scans were obtained from the Norman and Cimarron, Oklahoma, S-band Doppler radars over a 1-h period spanning the pretornadic phase of the storm. Using the dual-Doppler analysis technique contained in the NCAR software package CEDRIC (Mohr 1988), Dowell and Bluestein (1997) performed a detailed dual-Doppler analysis of this storm that will serve as our benchmark. Due to the lack of third radar, neither our nor Dowell and Bluestein's analysis can be validated against a more accurate analysis. Therefore, the discussion will remain qualitative.

The results of our analysis for 1634 CST on 17 May are shown in Fig. 12. At low levels (Fig. 12a), a cold outflow is seen to originate from rear-flank downdrafts that exhibit two maximum centers flanking the occlusion point of the gust fronts. Ahead of this outflow is the rear-flank gust front, which is associated with surface convergence and vertical velocity maximum. The reflectivity field shows a hook echo pattern that is consistent with the retrieved flow. Such a flow structure is
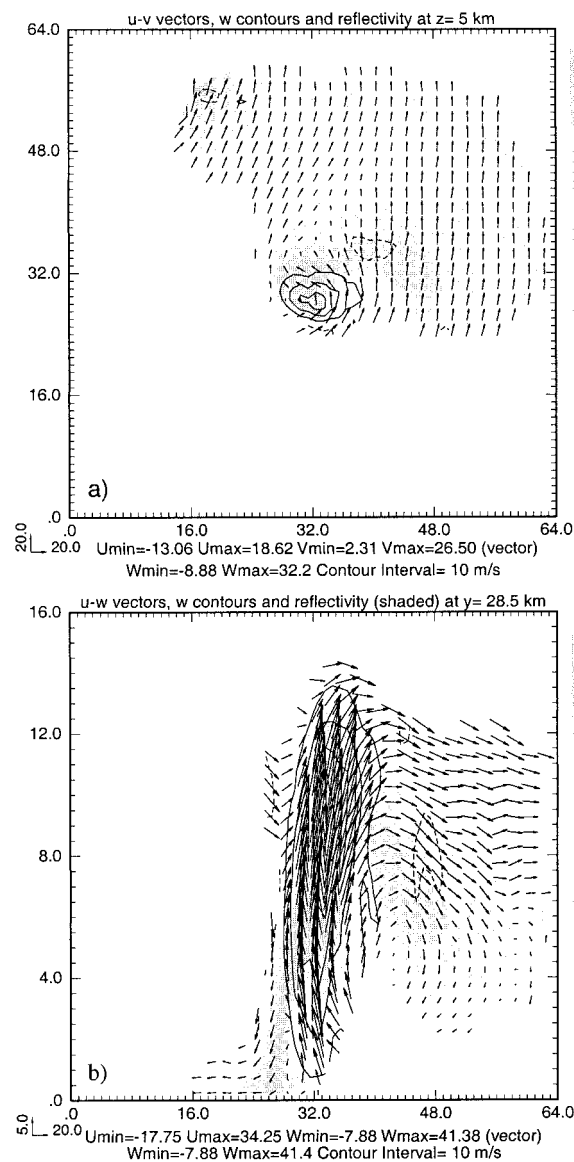
FIG. 10. Same as in Fig. 5 but for experiment ERR1, which includes random observational errors up to 20% of the original values.
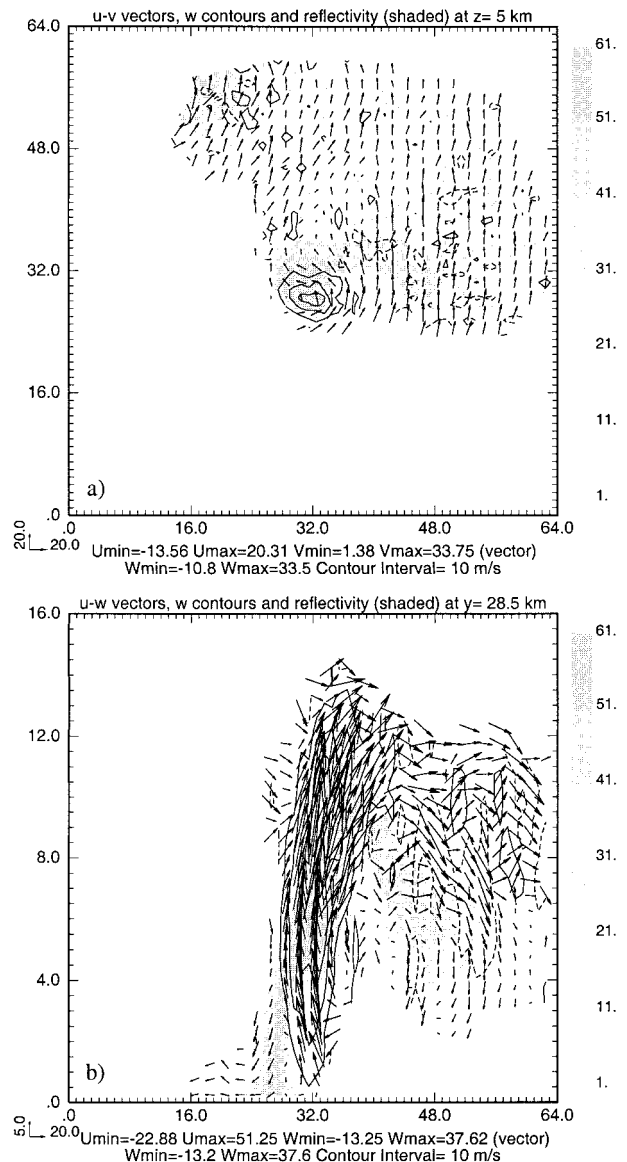
FIG. 11. Same as in Fig. 5 but for experiment ERR3, which includes random observational errors up to 100% of the original values.

typical of a tornadic supercell storm with strong low-level rotation (Lemon and Doswell 1979).

At midlevels, a strong updraft core (>25 m s^{-1}) is retrieved that is roughly collocated with the mesocyclone (center of strong rotation) and reflectivity maximum (Fig. 12b). In a vertical cross section plotted through the line A–B in Fig. 12a, the main updraft is seen to originate ahead of the low-level gust front. It reaches a maximum intensity of 35.42 m s^{-1} at the 8-km level and in general matches the areas of maximum reflectivity. The main downdraft is located below the updraft core and is collocated with a region of high reflectivity behind the gust front. These features suggest that both the horizontal and vertical flows are kine-matically consistent. They also qualitatively agree with those analyzed in Dowell and Bluestein (1997).

5. Summary and concluding remarks

In this paper, we proposed and tested a variational analysis scheme that is capable of retrieving three-dimensional winds from dual-Doppler observations of convective storms. It was shown that the variational method has notable advantages over traditional dual-Doppler analysis techniques. The need for explicitly integrating the mass continuity equations and solving elliptic equations in the variational adjustment step, as well as the "hole filling" procedure, makes the analysis
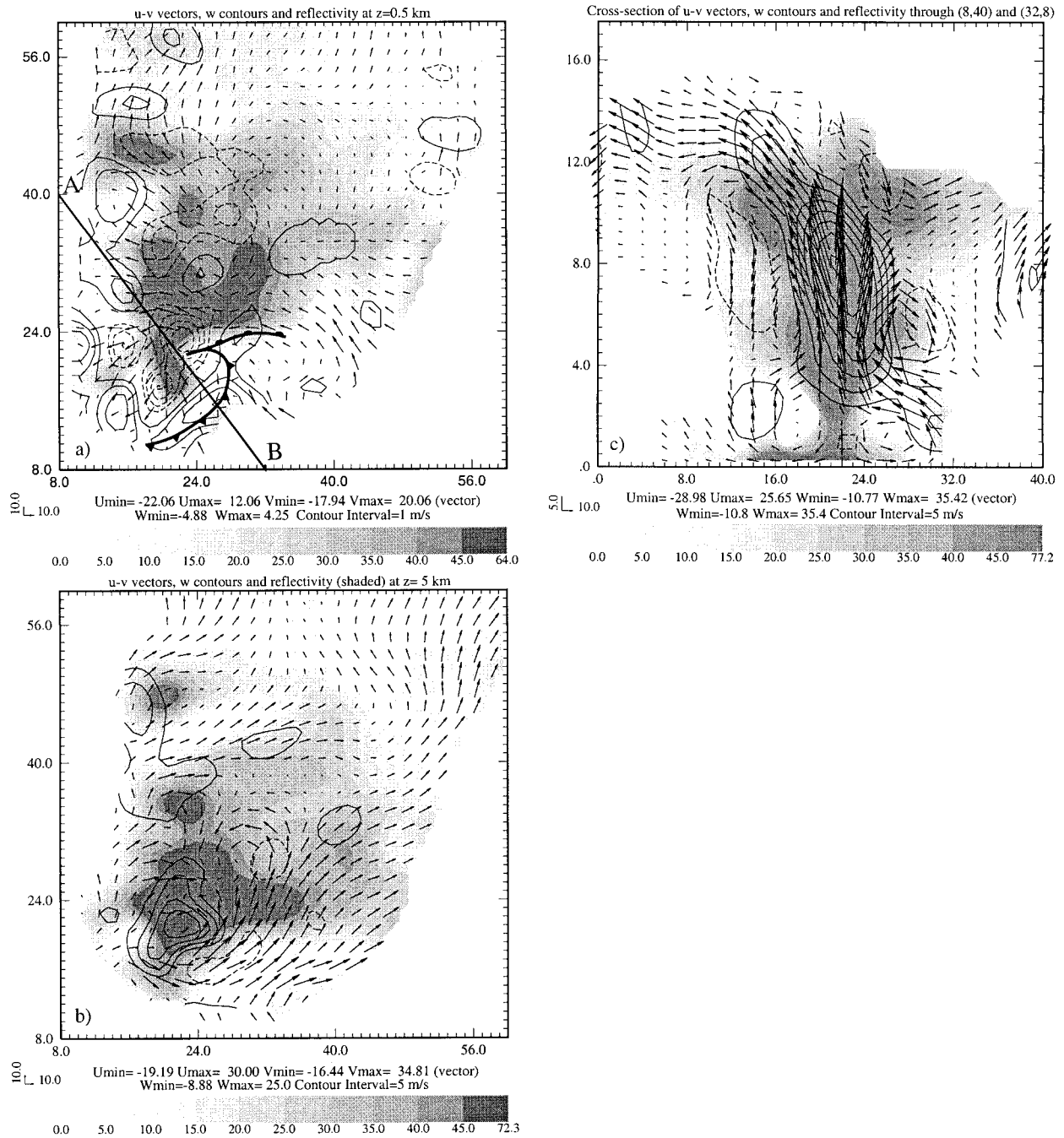
FIG. 12. Wind vectors and vertical velocity (contours) retrieved using the variational analysis method for the Arcadia, OK, 17 May 1981 tornadic storm. (a) Horizontal cross section at $z = 0.5$ km. (b) Horizontal cross section at $z = 5$ km. (c) Vertical cross section through line A–B in (a).

from traditional methods more susceptible to boundary condition uncertainties than the variational method here. In addition, separate interpolation from radar observation to an analysis grid in the traditional method is often a source of errors.

The main conclusions can be drawn as follows:

• The new method incorporates the radar data, and

background fields, along with smoothness, mass continuity, and possibly other dynamic constraints in a single cost function. By minimizing this cost function, an analysis with the desired fit to these constraints is obtained in a single step.

• Because the method preserves the radial nature of the observations, allowing for the backward interpolation

(from model grid to observation points) is used implicitly to keep the observations close to their ''raw'' form.

- The method is flexible in handling other types of data. They can be either analyzed and forecast background fields, or more conventional observations (e.g., surface mesonet, upper-air sounding and profile data). The use of a background naturally fills in the ''holes'' of radar observations. The method has the additional benefit of being able to retrieve, with reasonable accuracy, the fields from single-Doppler data, extending the effective area of analysis beyond that of traditional methods.
- Because no explicit integration of the anelastic mass continuity equation occurs, error accumulation during the integration is avoided. As a result, the method is also less sensitive to boundary uncertainties.
- The method is robust enough to resist large random observational errors.

We plan to generalize our variational analysis procedure to include additional data sources, and to introduce dynamic constraints in the cost function so that thermodynamical fields are retrieved simultaneously with the winds. This procedure is expected to further improve the wind analysis at the same time.

REFERENCES

Armijo, L., 1969: A theory for the determination of wind and precipitation velocities with Doppler radars. *J. Amos. Sci.,* **26,** 570–573.

Atkins, N. T., T. M. Weckwerth, and R. M. Wakimoto, 1995: Observations of the sea-breeze front during CaPE. Part II: Dual-Doppler and aircraft analysis. *Mon. Wea. Rev.,* **123,** 944–969.

Atlas, D., R. C. Srivastava, and R. S. Sekhon, 1973: Doppler radar characteristics of precipitation at vertical incidence. *Rev. Geophys. Space Phys.,* **11,** 1–35.

Brandes, E. A., 1977: Flow in severe thunderstorms observed by dual-Doppler radar. *Mon. Wea. Rev.,* **105,** 113–120.

Carbone, R. E., 1983: A severe frontal rainband. Part II: Tornado parent vortex circulation. *J. Atmos. Sci.,* **40,** 2639–2654.

Chong, M., J. Testud, and F. Roux, 1983a: Three-dimensional wind field analysis from dual-Doppler radar data. Part II: Minimizing the error due to temporal variation. *J. Climate Appl. Meteor.,* **22,** 1216–1226.

——, ——, and ——, 1983b: Three-dimensional wind field analysis from dual-Doppler radar data. Part III: The boundary condition: An optimum determination based on a variational concept. *J. Climate Appl. Meteor.,* **22,** 1227–1241.

Cressman, G. W., 1959: An operational objective analysis system. *Mon. Wea. Rev.,* **87,** 367–374.

Doviak, R. J., P. S. Ray, R. G. Strauch, and L. J. Miller, 1976: Error estimation in wind fields derived from dual-Doppler radar measurement. *J. Appl. Meteor.,* **15,** 868–878.

Dowell, D. C., and H. B. Bluestein, 1997: The Arcadia, Oklahoma, storm of 17 May 1981: Analysis of a supercell during tornadogensis. *Mon. Wea. Rev.,* **125,** 2562–2582.

Ellis, S., 1997: Hole-filling data voids in meteorological fields. M.S. thesis, University of Oklahoma, 198 pp. [Available from Bizzell Library, University of Oklahoma, Norman, OK 73019.]

Foote, G. B., and P. S. duToit, 1969: Terminal velocity of raindrops aloft. *J. Appl. Meteor.,* **8,** 249–253.

Gal-Chen, T., 1982: Errors in fixed and moving frame of references: Applications for conventional and Doppler radar analysis. *J. Atmos. Sci.,* **39,** 2279–2300.

Gao, J., J. Chou, and L. Zhi, 1995: A method for determining the spatial structure of meteorological variable from the temporal evolution of observational data. *Chinese J. Atmos. Sci.,* **19,** 113–125.

Gill, P. E., W. Murray, and M. H. Wright, 1981: *Practical Optimization.* Academic Press, 401 pp.

Hoffman, R. N., 1984: SASS wind ambiguity removal by direct minimization. Part II: Use of smoothness and dynamical constraints. *Mon. Wea. Rev.,* **112,** 1829–1852.

Kessinger, C. J., P. S. Ray, and C. E. Hane, 1987: The Oklahoma squall line of 19 May 1977. Part I: A multiple Doppler analysis of convective and stratiform structure. *J. Atmos. Sci.,* **44,** 2840–2864.

Kessler, E., 1969: *On the Distribution and Continuity of Water Substance in Atmospheric Circulation. Meteor. Monogr.,* No. 32, Amer. Meteor. Soc., 84 pp.

Klemp, J. B., and R. B. Wilhelmson, 1978: Simulations of right- and left-moving storms produced through storm splitting. *J. Atmos. Sci.,* **35,** 1097–1110.

——, and R. Rotunno, 1983: A study of the tornadic region within a supercell thunderstorm. *J. Atmos. Sci.,* **40,** 359–377.

——, R. B. Wilhelmson, and P. S. Ray, 1981: Observed and numerically simulated structure of a mature supercell thunderstorm. *J. Atmos. Sci.,* **38,** 1558–1580.

Lemon, L. R., and C. A. Doswell, 1979: Severe thunderstorm evolution and mesocyclone structure as related to tornadogenesis. *Mon. Wea. Rev.,* **107,** 1184–1197.

Lhermitte, R. M., and L. J. Miller, 1970: Doppler radar methodology for the observation of convective storms. Preprints, *14th Conf. on Radar Meteorology,* Tucson, AZ, Amer. Meteor. Soc., 133–138.

Lin, Y., P. S. Ray, and K. W. Johnson, 1993: Initialization of a modeled convective storm using Doppler radar-derived fields. *Mon. Wea. Rev.,* **121,** 2757–2775.

Miller, L. J., and R. G. Strauch, 1974: A dual Doppler radar method for the determination of wind velocities within precipitating weather systems. *Remote Sens. Environ.,* **3,** 219–235.

Mohr, C. G., 1988: CEDRIC—Cartesian Space Data Processor. NCAR, Boulder, CO, 78 pp.

Navon, I. M., and D. M. Legler, 1987: Conjugate-gradient methods for large-scale minimization in meteorology. *Mon. Wea. Rev.,* **115,** 1479–1502.

O'Brien, J. J., 1970: Alternative solutions to the classic vertical velocity problem. *J. Appl. Meteor.,* **9,** 197–203.

Parsons, D. B., and R. A. Kropfli, 1990: Dynamics and fine structure of a microburst. *J. Atmos. Sci.,* **47,** 1674–1692.

Ray, P. S., R. J. Doviak, G. B. Walker, D. Sirmans, J. Carter, and B.

Bumgarner, 1975: Dual-Doppler observations of a tornadic storm. *J. Appl. Meteor.,* **14,** 1421–1530.

——, C. L. Ziegler, W. Bumgarner, and R. J. Serafin, 1980: Single- and multiple-Doppler radar observations of tornadic storms. *Mon. Wea. Rev.,* **108,** 1607–1625.

——, B. C. Johnson, K. W. Johnson, J. S. Bradberry, J. J. Stephens, K. K. Wagner, R. B. Wilhelmson, and J. B. Klemp, 1981: The morphology of several tornadic storms on 20 May 1977. *J. Atmos. Sci.,* **38,** 1643–1663.

Reinking, R. F., R. J. Doviak, and R. O. Gilmer, 1981: Clear-air roll vortices and turbulent motions as detected with an air-borne gust probe and dual-Doppler radar. *J. Appl. Meteor.,* **20,** 678–685.

Sasaki, Y., 1970: Some basic formalisms in numerical variational analysis. *Mon. Wea. Rev.,* **98,** 875–883.

Shapiro, A., and J. J. Mewes, 1999: New formulations of dual-Doppler wind analysis. *J. Atmos. Oceanic Technol.,* **16,** 782–792.

Sun, J., and N. A. Crook, 1994: Wind and thermodynamic retrieval from single-Doppler measurements of a gust front observed during Phoenix II. *Mon. Wea. Rev.,* **122,** 1075–1091.

——, 1997: Dynamical and microphysical retrieval from Doppler radar observations using a cloud model and its adjoint. Part I: Model development and simulated data experiments. *J. Atmos. Sci.,* **54,** 1642–1661.

——, and ——, 1998: Dynamical and microphysical retrieval from Doppler radar observations using a cloud model and its adjoint.

Part II: Retrieval experiments of an observed Florida convective storm. *J. Atmos. Sci.,* **55,** 835–852.

Testud, J. D., and M. Chong, 1983: Three-dimensional wind field analysis from dual-Doppler radar data. Part I: Filtering, interpolation and differentiating the raw data. *J. Climate Appl. Meteor.,* **22,** 1204–1215.

Thacker, W. C., 1988: Fitting models to inadequate data by enforcing spatial and temporal smoothness. *J. Geophys. Res.,* **93,** 10 655–10 665.

Xu, Q., and C. J. Qiu, 1994: Simple adjoint methods for single-Doppler wind analysis with a strong constraint of mass conservation. *J. Atmos. Oceanic Technol.,* **11,** 289–298.

Xue, M., K. K. Droegemeier, V. Wong, A. Shapiro, and K. Brewster, 1995: Advanced Regional Prediction System (ARPS) version 4.0 user's guide. 380 pp. [Available from Center for Analysis and Prediction of Storms, University of Oklahoma, 100 E. Boyd, Norman, OK 73019.]

Yang, S., and Q. Xu, 1996: Statistical errors in variational data assimilation—A theoretical one-dimensional analysis applied to Doppler wind retrieval. *J. Atmos. Sci.,* **53,** 2563–2577.

Ziegler, C. L., 1978: A dual Doppler variational objective analysis as applied to studies of convective storms. M.S. thesis, University of Oklahoma, 116 pp. [Available from Bizzell Library, University of Oklahoma, Norman, OK 73019.]

——, P. S. Ray, and N. C. Knight, 1983: Hail growth in an Oklahoma multicell storm. *J. Atmos. Sci.,* **40,** 1768–1791.